Structural Basis of Mitochondrial Dysfunction in Response to Cytochrome *c* Phosphorylation at Tyrosine 48

Supplementary Information

Blas Moreno-Beltrán[1,*], Alejandra Guerra-Castellano[1,*], Antonio Díaz-Quintana[1], Rebecca Del Conte[2], Sofía M. García-Mauriño[1], Sofía Díaz-Moreno[3], Katiuska González-Arzola[1], Carlos Santos-Ocaña[4], Adrián Velázquez-Campoy[5], Miguel A. De la Rosa[1], Paola Turano[2] and Irene Díaz-Moreno[1,#]

[1]Instituto de Investigaciones Químicas, cicCartuja, Universidad de Sevilla – CSIC, Avda. Américo Vespucio 49, 41092 Seville (Spain).

[2]Magnetic Resonance Center (CERM) – Department of Chemistry, University of Florence, Via Luigi Sacconi 6, 50019 Sesto Fiorentino, Florence (Italy).

[3]Diamond Light Source Ltd., Harwell Science and Innovation Campus, Didcot, Oxfordshire OX11 0DE (United Kingdom).

[4]Centro Andaluz de Biología del Desarrollo, Universidad Pablo de Olavide – CSIC, and CIBERER Instituto de Salud Carlos III, Carretera de Utrera km. 1, 41013 Seville (Spain).

[5]Institute of Biocomputation and Physics of Complex Systems (BIFI), Joint Unit BIFI-IQFR (CSIC), Universidad de Zaragoza, Mariano Esquillor s/n, 50018 Zaragoza (Spain); Aragon Institute for Health Research (IIS Aragon), Avda. San Juan Bosco 13, 50009 Zaragoza, Spain; Fundacion ARAID, Government of Aragon, Maria de Luna 11, 50018 Zaragoza (Spain).

*These authors contribute equally to the work.

[#]Correspondence should be addressed to I. D.-M. (idiazmoreno@us.es)

Telephone number: +34 954489513; Fax number: +34 954460065

SUPPLEMENTARY METHODS

Protein expression and purification

Uniformly ^{13}C,^{15}N-labeled, ^{15}N-labeled and unlabeled samples of the Y48*p*CMF variant species of cytochrome *c* (C*c*)—in which tyrosine 48 was replaced by *p*-carboxymethyl-L-phenylalanine (*p*CMF)—were expressed using the evolved tRNA synthetase technique and purified as previously described (1, 2). For isotopic labelling, ^{15}N-labeled ammonium chloride and ^{13}C-labeled glucose were added to minimal cell culture media to express the ^{13}C,^{15}N-labeled protein samples, whereas only ^{15}N-labeled ammonium chloride was added to media for ^{15}N-labeled protein samples. Unlabeled *p*CMF and δ-aminolevulinic acid were added to a final concentration of 1 mM each after cell culture induction. Cultures were induced with IPTG and arabinose at 1 mM and 0.02% final concentrations, respectively. Tryptic digestion and MALDI-TOF analyses confirmed the molecular mass and the substitution of tyrosine by *p*CMF. Uniformly ^{15}N-labeled and unlabeled samples of wild-type (WT) C*c* were expressed and purified as reported previously (3). Protein concentration was determined by visible spectrophotometry, using an extinction coefficient of 29 mM^{-1} cm^{-1} for reduced Y48*p*CMF and WT C*c.* For NMR experiments, pure C*c* samples were first dialyzed against 10 mM sodium phosphate (pH 6.3), and afterwards concentrated in Millipore 3 K Nominal Molecular Weight Limit (NMWL) centricons until a final C*c* concentration of 0.7 mM.

Plant cytochrome c_1 (Cc_1) was obtained as described (4). Bovine cytochrome *c* oxidase (C*c*O) was purchased from Sigma; before use, the buffer was exchanged to 10 mM sodium phosphate buffer (pH 7.4), supplemented with 0.2% (w/v) *n*-dodecyl-β-D-maltoside (DDM) and 5 mM sodium dithionite, using Millipore 3K NMWL centricons, as reported previously (3).

Hypoxia-inducible domain family members 1A and 2A (HIGD1A and HIGD2A, respectively) were expressed by cell-free protein synthesis using a continuous exchange reaction

(dialysis mode; ratio 1:10), with a 6 mL final volume. Briefly, 10 μg mL^{-1} of either HIGD1A or HIGD2A-coding DNA in the pIVEX2.4d plasmid were added to the reaction mixture, which consisted of 1 mM amino acid mix, 0.8 mM ribonucleotides (guanosine-, uracyl- and cytidine-triphosphate), 1.2 mM adenosine triphosphate, 55 mM HEPES buffer (pH 7.5), 68 μM folinic acid, 0.64 mM cyclic adenosinemonophosphate, 3.4 mM dithiothreitol, 27.5 mM ammonium acetate, 2 mM spermidine, 80 mM creatine phosphate, 208 mM potassium glutamate, 16 mM magnesium acetate, 250 μg mL^{-1} of creatine kinase, 27 μg mL^{-1} of T7 RNA polymerase, 0.175 μg mL^{-1} of tRNA and 0.4 mL of S30 *Escherichia coli* (*E. coli*) bacterial extract. DDM detergent was added to a final concentration of 0.4% (w/v). For the feeding mix in the external tank (60 mL), the same conditions were used but omitting DNA, creatine kinase, T7 RNA polymerase, tRNA and S30 *E. coli* bacterial extract. Incubation was carried out at 23°C with agitation for 16 h. The His-tagged forms of HIGD1A and HIGD2A were then purified by nickel affinity chromatography. The final yield was 125 μg of protein per mL of reaction in both cases. Before using the HIGD proteins, the buffers were exchanged to 10 mM sodium phosphate buffer (pH 7.4) with 0.2% (w/v) DDM.

Circular dichroism

Circular dichroism (CD) spectra were recorded on a JASCO J-815 spectropolarimeter, equipped with a Peltier temperature system, in a 1-mm quartz cuvette. CD intensities were presented in terms of molar ellipticity [θ_{molar}], based on molar protein concentration (5). Secondary structural elements of reduced WT and Y48*p*CMF C*c* were analyzed by recording their respective far-UV CD spectra (185–250 nm) at 25°C. The samples contained 3 μM hemeprotein in 5 mm sodium phosphate buffer (pH 6.3), supplemented with 10 mM ascorbic acid. Twenty scans were averaged and analyzed for each sample, using the CDPro

software package (6, 7) SMP50 and SP37A were used as reference sets. CLSTR option was employed for comparison with a set of proteins with similar folds.

Nuclear magnetic resonance experiments

Nuclear magnetic resonance (NMR) spectra of fresh 0.6 mM reduced ^{13}C,^{15}N-labeled Y48*p*CMF C*c* samples, in 90% buffer and 10% D_2O, were recorded at 25 °C on Bruker Avance spectrometers operating at 950, 700 and 500 MHz ^{1}H frequencies. A standard set of triple-resonance experiments, necessary for the full assignment of backbone and side-chain resonances, were acquired at 700 MHz ^{1}H frequency, whereas 2D and 3D NOESY experiments required for structure determination were acquired at 950 MHz ^{1}H frequency. Recorded NMR experiments for determination of backbone resonances were 2D ^{1}H-^{15}N heteronuclear single-quantum correlation (HSQC), 2D ^{1}H-^{13}C HSQC, 3D HNCA, 3D HNCACB, 3D CACB(CO)NH, 3D HN(CA)CO and 3D HNCO, and specific experiments for determination of side-chain resonances were 3D HCCHTOCSY and 3D HBHA(CO)NH (8-10). Additional 2D COSY and aromatic 2D ^{1}H-^{13}C HSQC spectra of an unlabeled sample of Y48*p*CMF C*c* were acquired for the assignment of aromatic residues. Therefore, the ^{1}H-^{13}C HSQC spectrum was recorded in natural abundance of ^{13}C. Water suppression was achieved in all mentioned spectra by WATERGATE (11) 1D ^{1}H spectra were launched before and after each spectrum to check the state of the sample, and especially the redox state of the hemeprotein.

The following NOESY experiments were acquired: 2D ^{1}H-^{15}N NOESY, 3D ^{1}H-^{15}N NOESY-HSQC and 3D ^{1}H-^{13}C NOESY-HSQC spectra in the aliphatic region (12-14). Mixing times were 100 ms for all NOESY experiments, recorded on a ^{15}N-labeled sample, with the exception of the 3D ^{1}H-^{13}C NOESY-HSQC, which was acquired on a ^{13}C,^{15}N-labeled sample. An additional 2D ^{1}H-^{15}N EXSY spectrum was launched for assignment of heme resonances

using a partially oxidized ^{15}N-labeled sample. WATERGATE suppression was used. 1D ^{1}H spectra were again launched to check the state of the samples.

^{15}N relaxation R_1 (=1/T_1), R_2 (=1/T_2) and {^{1}H}-^{15}N NOE parameters (also known as HetNOE) were obtained from standard experiments recorded at 500 MHz ^{1}H frequency and 25 °C (15) on ^{15}N-labeled samples of the Y48*p*CMF and WT C*c* species. R_1 and R_2 values were obtained using 10 delays, of 1, 2.5, 10, 35, 70, 200, 380, 550, 740 and 3000 ms for R_1 experiments, and 16.96, 33.92, 67.84, 101.76, 135.68, 186.56, 237.44, 271.36, 305.28 and 356.16 ms for R_2 experiments. To determine HetNOE values, spectra were recorded in the presence or absence of a proton presaturation period. HetNOE, R_1 and R_2 values from residues in well-defined regions were used to estimate the comprehensive ^{15}N relaxation parameters (16, 17). The R_1/R_2 ratio was used to estimate the rotational correlation time (τ_c) of the protein constructs using TENSOR2 software (17). Internal mobility was also calculated by an isotropic model-free analysis via TENSOR2 routines (17). Amide hydrogen exchange experiments were also carried out on these ^{15}N-labeled samples of the Y48*p*CMF and WT C*c* species. For this purpose, 2D ^{1}H-^{15}N HSQC experiments were run using C*c* samples in 95% buffer and 5% D_2O, or 100% D_2O.

NMR data processing was carried out using the Bruker TopSpin software package. The assignments of 2D and 3D spectra were performed manually with the help of the CARA and SPARKY software packages (18, 19). A list of NOEs of reduced yeast C*c* was used as a reference (20). Final reviews of peak assignments and integrations of peak volumes were executed by the XEASY software (21). ^{15}N relaxation parameters were analyzed using CARA routines (19).

NMR titrations of 100 μM ^{15}N-labeled, reduced Y48*p*CMF C*c* with aliquots of unlabeled, reduced plant cytochrome c_1 (Cc_1) were performed at 25ºC and recorded on a Bruker Avance 700 MHz. Titrations were performed in 5 mM sodium phosphate (pH 6.3) with 10%

D_2O. Each titration step was prepared in an independent NMR tube (Shigemi) up to a 0.28 mL final volume. The pH of the samples was checked before and after recording each spectrum. The Chemical-Shift Perturbations (CSP) were monitored in a series of ^{1}H-^{15}N HSQC experiments. The data were processed using Bruker TopSpin and analyzed with SPARKY (18). CSP titration curves were analyzed with Origin 7 (OriginLab, http://www.originlab.com), using a two-parameter non-linear least squares fit with two-site binding model, as previously described (3, 4).

Distance geometry calculations

Volumes of cross-peaks between assigned resonances were obtained using the integration routines of the XEASY program. Elliptical integration was applied. NOESY cross-peak intensities were converted into upper limits of inter-atomic distances by CYANA (22). The heme group, axial ligands and two Cys residues covalently linked to the porphyrin ring were treated as in previous computations (23). Upper and lower distance limits were imposed to build up the heme group. Upper (1.90 Å) and lower (1.70 Å) distance limits from the α-carbons of thioethers 2 and 4 of the heme moiety to the S_γ of cysteines 14 and 17, respectively, were used in the computations to covalently link the heme moiety to the cysteine residues. An upper distance limit of 2.50 Å and a lower distance limit of 2.20 Å between the S_δ of Met80 and the heme iron atom were also introduced. The orientations of Met80 and His18 side-chains were defined only by experimental NOE constraints.

A residue containing the heme moiety was added to the standard CYANA library. In addition, the non-standard amino acid *p*CMF was built and added to the CYANA library. Several cycles of structure calculation were carried out in order to recalibrate the NOE distance constraints. CYANA calculations were performed following the procedure and with the parameters used for the determination of other *c*-type cytochromes (20, 24, 25). Initially, 200

structures were calculated. In each calculation, violated constraints were analyzed for the 20 best structures with respect to the target function. After consecutive rounds of review and refinement of violated constraints, a final CYANA computation was performed in which no consistent violations were determined. The final average value of the target function was equal to 0.73 ± 018.

Molecular dynamics simulations

NMR-restrained Molecular Dynamics (RMD) computations were performed by the AMBER 12.1 package and using the AMBER-2003 force field on a selection of the 20-best structures derived from the CYANA calculations (26, 27). Distance constraints were introduced by the DIS_RST module of Amber 12.1. Simulations were performed under periodic boundary conditions using an orthorhombic cell geometry (with the minimum distance between protein and cell faces initially set to 10 Å) and particle mesh Ewald (PME) electrostatics with a Ewald summation cut off of 9 Å. The structures were solvated with extended simple point charge model (SPC) water molecules, and Cl^- counterions were added to neutralize the net charge of the full systems. Afterwards, solvent and counterions were subjected to 2500 steps of steepest descent minimization followed by 500 ps NPT-MD computations using isotropic molecule position scaling and a pressure relaxation time of 2 ps at 298 K. Once the systems were NMR-restrained energy minimized (REM), the resulting data were submitted to RMD computations for 5 ns at 298 K. The temperature was regulated using a Langevin thermostat with a collision frequency of 5 ps^{-1} (28). Finally, structures from RMD were energy minimized for 5000 steps. The SHAKE algorithm was used to constrain bonds involving hydrogen atoms (29). The PTRAJ module of AMBER was used for trajectory analyses. Force field parameters for the heme group were taken from a previous work (30). The Met80 residue was non-bonded to the iron atom and a constraint was applied instead. Molecular graphics

were performed with UCSF Chimera (31). Final minimized structures were validated by the Protein Structure Validation Software suite (PSVS) (32), the iCING server (33) and the Protein Data Bank (PDB) validation suite. In addition, a non-restrained MD computation of 20 ns was launched to check the stability of the resulting conformers. A non-restrained MD computation of 20 ns was also launched on the NMR structure of WT C*c*. S^2 parameters values per residue were obtained from the non-restrained computations performed for both C*c* species.

Finally, NMR assignments and PDB coordinates for the Y48*p*CMF C*c* were deposited in the Biological Magnetic Resonance Data Bank (BMRB) and PDB databases. BMRB and PDB entries for the Y48*p*CMF C*c* are 25660 and 2N3Y, respectively.

X-ray absorption spectroscopy

X-ray absorption spectroscopy (XAS) experiments were carried out at Diamond Light Source (UK), operating at 3 GeV and 300 mA ring current. The Fe K-edge (7112 eV) was measured at beamline I20-scanning, comprising a four-bounce Si(111) crystal monochromator. Two Rh-coated mirrors working at 5.0 mrad were used for high-energy harmonics rejection. The spectra were recorded in fluorescence mode, using a 36-element monolithic Ge detector (Canberra). An iron foil was simultaneously recorded in transmission mode using ionization chamber detectors to be used as internal calibration. To avert radiation damage, X-rays were attenuated with a 1.5-mm thick carbon foil. In addition, samples were measured at cryogenic temperatures using a liquid nitrogen cryojet (Oxford Instrument). Each datapoint was collected using a 1 s acquisition time, and 36 scans were averaged. Samples were measured in plastic capillary cells. 350 μM reduced C*c* samples were prepared in 10 mM sodium phosphate buffer (pH 5.8).

Spectra averaging, background subtraction and amplitude normalization required to obtain the extended X-ray absorption fine structure (EXAFS) signals (k) were performed using the Athena (version 0.9.024) code (34). The best fit to the data was performed by using the Artemis program (version 0.9.024) (34). Scattering paths were computed using FEFF 6.0. Initial atomic coordinates of the heme moiety were taken from the crystallographic structure of the WT form (PDB: 3zcf) (35). Neither the initial coordinates from this structure nor those from the NMR structure (PDB: 1j3s) (36) yielded acceptable fits. Still, the distances coming out from these fits were used as input to screen 10^4 coordinates from each MD computation (2). The snapshots with the smallest sum of quadratic distance differences with respect to the EXAFS fit-derived distances were selected iteratively.

Isothermal titration calorimetry

Interactions of the human C*c* species with plant Cc_1, at their reduced and oxidized states were analyzed by isothermal titration calorimetry (ITC) using an Auto-ITC200 microcalorimeter (MicroCal) at 25 °C. The reference cell was filled with distilled water. The experiments consisted of 2 μL injections of 0.4 mM C*c* solution in 10 mM sodium phosphate buffer (at pH 5.8, 7.4 and 8.5) into the sample cell, initially containing 20 μM Cc_1 solution in the same buffer. All solutions were degassed before titration. Titrant was injected at appropriate time intervals to ensure that the thermal power signal returned to the baseline prior to the next injection. To achieve a homogeneous mixing in the cell, the stirring speed was kept constant at 1000 rpm. The data, specifically the heat-per-injection normalized per mol of injectant *versus* molar ratio, were analyzed with Origin 7 (OriginLab) using a two-site binding model with a distinct affinity for each site, as recently reported for the plant C*c*-Cc_1 complex (4). In addition, the titration of reduced bovine C*c*O (3.85 μM) with the reduced C*c* species (0.10 mM) was performed in 10 mM sodium phosphate buffer (pH 7.4),

supplemented with 0.2% (w/v) *n*-dodecyl-β-D-maltoside and 5 mM sodium dithionite, as described previously (3). ITC experiments were repeated at least twice to confirm that the data were consistent. The titration of C*c* onto buffer containing detergent yielded small invariable injection heats attributed to dilution. Calibration and performance tests of the calorimeter were carried out by conducting Ca^{+2}-EDTA titrations with the solutions provided by the manufacturer.

ITC assays were analyzed considering several models: single binding site, two identical independent binding sites and two different independent binding sites.

Single binding site

A single binding site for C*c* is considered in Cc_1 (or C*c*O). The total concentration of C*c* and Cc_1 (or C*c*O) in the cell after injection *i* was calculated as:

$$[\mathrm{C}c]_{T,i} = [\mathrm{C}c]_0 \left(1 - \left(1 - \frac{v}{V_0}\right)^i\right)$$

$$[\mathrm{C}c1]_{T,i} = [\mathrm{C}c1]_0 \left(1 - \frac{v}{V_0}\right)^i$$

where $[\mathrm{C}c]_0$ and $[\mathrm{C}c_1]_0$ are the concentrations of C*c* in the syringe and the initial concentration of Cc_1 (or C*c*O) in the cell, v is the injection volume, and V_0 is the cell volume. Mass conservation principle and chemical equilibrium allow writing a set of coupled equations for C*c* and Cc_1 (or C*c*O):

$$[\mathrm{C}c]_T = [\mathrm{C}c] + [\mathrm{C}c1{:}\,\mathrm{C}c] = [\mathrm{C}c] + K_A[\mathrm{C}c1][\mathrm{C}c]$$
$$[\mathrm{C}c1]_T = [\mathrm{C}c1] + [\mathrm{C}c1{:}\,Cc] = [\mathrm{C}c1] + K_A[\mathrm{C}c1][Cc]$$

where K_A is the equilibrium association constant for the complex Cc_1:C*c* (or C*c*O:C*c*). These two equations can be transformed into a single equation in [C*c*]:

$$[\mathrm{C}c]_T = [\mathrm{C}c] + [\mathrm{C}c1]_T \frac{K_A[\mathrm{C}c]}{1 + K_A[\mathrm{C}c]}$$

which is a quadratic polynomial equation that can be solved at each experimental point in the calorimetric titration in order to find the concentration of free C*c*. Then, the concentration of complex Cc_1:C*c* (or C*c*O:C*c*) after each injection can be calculated:

$$[\mathrm{C}c1{:}\,\mathrm{C}c] = [\mathrm{C}c1]_T \frac{K_A[\mathrm{C}c]}{1 + K_A[\mathrm{C}c]}$$

Finally, the titrant-normalized heat effect associated with each injection *i* can be calculated from the net increase of complex Cc_1:C*c* (C*c*O:C*c*) or concentration along injection *i*:

$$q_i = \frac{V_0}{v[\mathrm{C}c]_0} \Delta H \left([\mathrm{C}c1{:}\,Cc]_i - [\mathrm{C}c1{:}\,Cc]_{i-1} \left(1 - \frac{v}{V_0}\right)^i \right) + q_d$$

where ΔH is the interaction enthalpy, and q_d is an additional parameter accounting for the background (or dilution) heat. Non-linear least-square regression analysis of the experimental data using the previous equation provides an estimation of the binding parameters.

Two independent binding sites

Two independent binding sites for C*c* are considered in in Cc_1 (or C*c*O). The total concentration of C*c* and in Cc_1 (or C*c*O) in the cell after injection *i* was calculated as:

$$[\mathrm{C}c]_{T,i} = [\mathrm{C}c]_0 \left(1 - \left(1 - \frac{v}{V_0}\right)^i\right)$$

$$[\mathrm{C}c1]_{T,i} = [\mathrm{C}c1]_0 \left(1 - \frac{v}{V_0}\right)^i$$

where $[\mathrm{C}c]_0$ and $[\mathrm{C}c_1]_0$ are the concentration of Cc in the syringe and the initial concentration of Cc_1 (or C*c*O) in the cell, v is the injection volume, and V_0 is the cell volume. Mass conservation principle and chemical equilibrium allow writing a single equation in [C*c*]:

$$[\mathrm{C}c]_T = [\mathrm{C}c] + [\mathrm{C}c1]_T \left(\frac{K_{A1}[\mathrm{C}c]}{1 + K_{A1}[\mathrm{C}c]} + \frac{K_{A2}[\mathrm{C}c]}{1 + K_{A2}[\mathrm{C}c]} \right)$$

where K_{A1} and K_{A2} are the equilibrium association constants for the complexes Cc_1:C*c* (or C*c*O:C*c*) and C*c*:Cc_1 (or C*c*:C*c*O). This is a cubic polynomial equation that can be solved (numerically) at each experimental point in the calorimetric titration in order to find the

concentration of free C*c*. Then, the concentration of complexes Cc_1:C*c* (or C*c*O:C*c*) and C*c*:Cc_1 (or C*c*:C*c*O) after each injection can be calculated:

$$[\mathrm{C}c1{:}\,\mathrm{C}c] = [\mathrm{C}c1]_T \frac{K_{A1}[\mathrm{C}c]}{1 + K_{A1}[\mathrm{C}c]}$$

$$[\mathrm{C}c{:}\,\mathrm{C}c1] = [\mathrm{C}c1]_T \frac{K_{A2}[\mathrm{C}c]}{1 + K_{A2}[\mathrm{C}c]}$$

Finally, the titrant-normalized heat effect associated with each injection *i* can be calculated from the net increase of complexes Cc_1:C*c* (or C*c*O:C*c*) and C*c*:Cc_1 (or C*c*:C*c*O) concentration along injection *i*:

$$q_i = \frac{V_0}{v[\mathrm{C}c]_0}\left(\Delta H_1\left([\mathrm{C}c1{:}\,\mathrm{C}c]_i - [\mathrm{C}c1{:}\,\mathrm{C}c]_{i-1}\left(1 - \frac{v}{V_0}\right)^i\right)\right.$$

$$\left. + \Delta H_2\left([\mathrm{C}c{:}\,\mathrm{C}c1]_i - [\mathrm{C}c{:}\,\mathrm{C}c1]_{i-1}\left(1 - \frac{v}{V_0}\right)^i\right)\right) + q_d$$

where ΔH_1 and ΔH_2 are the interaction enthalpies for each binding site. Non-linear least-square regression analysis of the experimental data using the previous equation provides estimates of the binding parameters.

This model corresponds to *two identical independent binding sites* when it is imposed that $K_{A1} = K_{A2}$ and $\Delta H_1 = \Delta H_2$.

C-values calculated using the K_D values of the *proximal* site in the Y48*p*CMF C*c*-involving titrations (Tables S5 and S6) are in the range of values allowed ($1 < C < 1000$).

Calorimetric liposome binding assays were carried out in a low-volume Nano-ITC (TA instruments, Inc.). All titrations were performed in 25 mM HEPES buffer (pH 7.4). A 6 μM C*c* solution, previously reduced by an excess of sodium ascorbate that was further removed by dialysis, was titrated with a suspension of unilamellar liposomes. Stirring was set to 350 rpm. Unilamellar liposomes contained 1,2-dioleoyl-*sn*-glycero-3-phosphocholine (DOPC) either alone or with 1,1'2,2'-tetraoleoylcardiolipin (TOCL) at a 4:1 ratio. Total lipid concentration in

the syringe was 8.9 mM. DOPC unilamellar liposomes (7.9 mM) were used for control experiments. All ITC samples were previously degassed allowing C*c* species to remain reduced in the syringe. In addition, C*c*-liposome binding assays were performed under aerobic conditions, as reported in ref. (37). In such binding assays, each liposome could accommodate several C*c* molecules. Data processing and analyses were carried out with the Nanoanalyze software (TA Instruments).

Cytochrome *c* oxidase assays

The ability of C*c* species to act as electron donors for cytochrome *c* oxidase (C*c*O) activity was tested in isolated complex IV and in mitochondria from *Saccharomyces cerevisiae*. Two yeast cell strains were used for mitochondria extraction, namely WT (BY4741; MATa; ura3Δ0; leu2Δ0; his3Δ1; met15Δ0) (WT_{mito}) and C*c*-deficient Y06846 (BY4741; MATa; ura3Δ0; leu2Δ0; his3Δ1; met15Δ0; YJR048w::kanMX4) (Δ*Cc*) strains. Two other yeast cell strains were likewise used for mitochondria extraction, namely WT (W303-1A; mata leu2 trp1 ura3 his3 ade2) (WT_{Rcf}) and Rcf-deficient RCF1::HIS3 RCF2::KAN (W303-1A; mata leu2 trp1 ura3 ade2) (ΔRcf1/2) strains. WT_{mito} and Δ*Cc* cells were grown in YPD medium (1% yeast extract, 2% peptone and 2% glucose), whereas WT_{Rcf} and ΔRcf1/2 cells were grown in YPD medium or YP-0.5% lactate medium supplemented with 2% galactose (YP-Gal), as described previously (38), to obtain mitochondria-enriched cells. In all cases, crude mitochondria were isolated as previously described (39) and stored at –80^{o}C in 0.6 M sorbitol, 20 mM K-MES buffer (pH 6.0). The C*c*O activity was measured spectrophotometrically (Beckman DU® 650 spectrophotometer) using the commercial C*c*O activity kit from Sigma®, according to the manufacturer's instructions. The kit uses a colorimetric assay based on observation of the decrease in absorbance at 550 nm caused by oxidation of ferro-C*c* to ferri-C*c* by C*c*O. The WT and Y48*p*CMF recombinant forms of

human C*c* herein used (rather than C*c* provided with the Sigma kit) were used. It was also tested that endogenous C*c* from WT_{mito}, WT_{Rcf} and ΔRcf1/2 mitochondria did not affect the C*c*O assay. To facilitate the interpretation of experimental findings, the relative C*c*O activities were represented upon normalization of the data obtained with Y48*p*CMF to those with WT C*c*. In experiments with HIGD1A/2A proteins, the reaction mixtures were incubated at 25 ºC for 30 min before running the assay. Oxygen consumption rates were measured with an Oxygraph system (Hansatech) in the presence of 1 mM sodium ascorbate. A control trace (C*c*O in the presence of sodium ascorbate) was subtracted from the experimental data.

Liposome preparation and binding experiments

In order to analyze the interaction of the reduced C*c* species with cardiolipin (CL), small unilamellar liposomes were prepared by sonication in 25 mM HEPES buffer (pH 7.4). Liposomes contained either DOPC and TOCL (4:1 ratio) or DOPC alone (manufactured by Avanti Polar Lipids®). The diameter of liposomes was 27.5 ± 10.8 nm, as inferred by Dynamic Light Scattering measurements. C*c*:liposome binding assays were performed by incubating the C*c* species with DOPC or TOCL/DOPC liposomes at different ratios (protein:lipids) for 1 h in 25 mM HEPES buffer (pH 7.4). The complexes were analyzed by electrophoretic mobility shift assay (EMSA). The samples were applied onto 0.8% agarose gel, and the electrophoresis was run for 90 min at 50 V in non-denaturing 35 mM HEPES buffer (pH 7.4). Gels were stained for protein detection with 0.25% Coomassie Brilliant Blue R-250 in 45% methanol and 10% acetic acid.

Peroxidase assays

Peroxidase assays of C*c*:liposomes were performed as previously described with minor modifications (40). TOCL/DOPC liposomes were incubated for 1 h at room temperature with

reduced C*c* (1 μM) in a 1:100 ratio (w/w) (protein:lipid) in 20 mM HEPES buffer (pH 7.4). After incubation, and immediately before starting the measurement, 2′,7′-dichlorofluorescin diacetate (H_2DCF) and H_2O_2 were added to the samples at 5 μM and 100 μM final concentrations, respectively. Increases in DCF fluorescence at 522 nm were recorded along 30 min upon excitation at 502 nm, with 5-nm slits, in a Cary Eclipse (Varian) fluorescence spectrophotometer. Basal peroxidase activity of C*c* in CL-free liposomes was used as control.

Caspase activation assays

In vitro activation of caspases was achieved as described previously with minor modifications (41). Human embryonic kidney 293 (HEK 293) cytoplasmic cell extract (100 μg), prepared as described previously (42), was incubated for 60 min at 37°C, in a total volume of 25 μL, with 25 mM KCl, 0.2 mM DTT, 0.2 mM dATP and human WT or Y48*p*CMF C*c* at a final concentration of 8 μM. After incubation, 180 μL of buffer A (10 mM HEPES buffer (pH 7.0) with 50 mM NaCl, 40 mM β-glycerophosphate, 2 mM $MgCl_2$, 5 mM EGTA, 0.1 mg mL^{-1} bovine serum albumin, and 0.1% (w/v) CHAPS), supplemented with 10 μM of acetyl-Asp-Glu-Val-Asp-7-amino-4-methylcoumarin (Ac-DEVD-AMC; a fluorescent substrate specific for caspases 3/7), was added to the reaction mixture. Fluorescence increases resulting from Ac-DEVD-AMC cleavage was rapidly determined in a Cary Eclipse (Varian) fluorescence spectrophotometer (optical slits of 2.5 nm), using an excitation wavelength of 360 nm and an emission wavelength of 460 nm. Data were the averages of at least three independent experiments.

Blue-native gel electrophoresis of protein complexes from yeast mitochondria

Fresh mitochondria (400 µg of protein) isolated from yeast cell extracts were permeabilized in 40 µL of solubilization buffer (30 mM HEPES buffer (pH 7.4), with 150 mM KOH-acetate, 10% glycerol and 1 mM PMSF) plus digitonin at a 4:1 (w:w) ratio of digitonin:protein. Samples were incubated on ice for 30 min, centrifuged for 30 s, and loaded onto NativePAGE Novex 3–12% Bis-Tris protein gel (1.0 mm, 15-well; Thermo Fisher Scientific, cat. No. BN2012BX10), following the manufacturer's instructions.

Antibodies

Mouse monoclonal anti-His_6 and anti-α-tubulin were obtained from Sigma-Aldrich (catalog numbers 11922416001 and T8328, respectively). Secondary horseradish peroxidase (HRP)-conjugated anti-mouse IgG was obtained from Sigma-Aldrich (catalog number A4416). Rabbit antibody against yeast C*c*, and mouse antibody again yeast COX II, were a gift from Dr. Carlos Santos-Ocaña. Rabbit antibodies against the C-terminal domains of yeast Rcf1 and Rcf2 were kindly provided by Prof. Peter Rehling. Rabbit antiserum against yeast Cc_1 was a gift from Prof. Nikolaus Pfanner. Rabbit anti-human C*c* serum was obtained by immunizing male rabbits with full-length recombinant C*c* suspended in a 0.85% NaCl solution. Secondary horseradish peroxidase (HRP)–conjugated anti-rabbit IgG was obtained from Sigma-Aldrich (catalog number A0545).

Western blot analysis

For immunoblot detection of yeast C*c*, Rcf1 and Rcf2 in mitochondria and human C*c* and α-tubulin in cytoplasmic fractions of HEK293 cells, protein quantification was first assessed using the Bradford protein assay (43). For immunodetection of Cc_1, COX II, Rcf1 and Rcf2 inside the respiratory supercomplexes, mitochondrial content were obtained after permeabilization and protein quantification by the Bradford protein assay (43). For

cytoplasmic cell extracts and mitochondria samples, 10–20 μg of proteins were resolved by β-dodecyl sulphate–polyacrylamide gel electrophoresis (SDS-PAGE). For supercomplexes analysis, 20-μg protein samples were loaded onto NativePAGE Novex 3–12% Bis-Tris protein gels (1.0 mm, 15-well; Thermo Fisher Scientific, catalog number BN2012BX10), which were further transferred to polyvinylidene fluoride (PVDF) membranes (EMD Millipore) using a Mini Trans-Blot electrophoretic transfer cell (Bio-Rad). Membranes were blocked in 5% nonfat dry milk in PBS with Tween-20 (TPBS) for cytoplasmic extracts and mitochondria, and in only TBS for supercomplex analyses. Immunoblots were performed with primary antibodies, and then HRP-conjugated secondary antibodies were used for detection. The immunoreactive bands were detected using Amersham ECL Plus Western Blotting Detection Reagents (GE Healthcare Life Sciences).

SUPPLEMENTARY TABLES

Table S1. **NMR experiments performed on reduced Y48*p*CMF C*c***

	Experiments	Magnetic Field
Backbone assignment	2D ^{1}H-^{15}N HSQC, 2D ^{1}H-^{13}C HSQC, 3D HNCA, 3D HNCACB, 3D CBCA(CO)NH, 3D HN(CA)CO and 3D HNCO.	700 MHz
Side-chain assignment	2D ^{1}H-^{13}C HSQC, 2D COSY, 3D HBHA(CO)NH and 3D HCCH-TOCSY.	700 MHz
	Aromatic 2D ^{1}H-^{13}C HSQC	500 MHz
Mobility analysis	^{15}N R_1, ^{15}N R_2 and steady-state {^{1}H}-^{15}N NOE	500 MHz
Distance constraints	2D ^{1}H-^{1}H NOESY, 3D ^{1}H-^{15}N NOESY-HSQC, 3D ^{1}H-^{13}C NOESY-HSQC	950 MHz
Heme assignments & constraints	2D COSY, 2D ^{1}H-^{15}N NOESY and ^{1}H-^{15}N EXSY	950 MHz
Amide hydrogen exchange	2D ^{1}H-^{15}N HSQC	700 MHz
Biomolecular interactions	2D ^{1}H-^{15}N HSQC	700 MHz

Table S2. NMR statistics of the Y48*p*CMF C*c* structure

NMR distance and dihedral constraints	
Distance constraints	
Total meaningful NOE	2,176
Intra-residue	360
Inter-residue	1,816
Sequential ($\|i - j\| = 1$)	763
Medium-range ($\|i - j\| \leq 5$)	539
Long-range ($\|i - j\| > 5$)	514
Total dihedral angle restraints	
ϕ	71
ψ	71
Structure statistics	
Violations	
Average target function	0.73 ± 0.18
Distance constraints (Å)	0.0059 ± 0.0014
Dihedral angle constraints (º)	0.3336 ± 0.0973
Max. distance constraint violation (Å)	0.29
Max. dihedral angle violation (º)	3.79
RMSD of minimized 20 conformers to the mean (Å)	
Backbone	0.89 ± 0.01
Heavy atoms	1.33 ± 0.24
Global RMSD of minimized 20 conformers (Å)	
Backbone	1.28 ± 0.30
Heavy atoms	1.91 ± 0.38
Ramachandram plot statistics from Procheck	
Residues in favoured regions (%)	98.80 ± 0.10
Residues in generously allowed regions (%)	1.00 ± 0.10
Residues in disallowed regions (%)	0.20 ± 0.10
Global quality	
Procheck G-factor (all dihedrals, raw score)	-0.436 ± 0.046
Verify 3D	0.432 ± 0.030
Prosall	0.578 ± 0.047
MolProbity Clashscore	2.564 ± 1.263
Number of close contacts	0
Deviations from ideal bond distance (Å)	0.013 ± 0.001

Table S3. EXAFS fits of the Y48*p*CMF C*c* structure

	Paths	σ^2_{path} (Å²)	R (Å)	ΔE_0 (eV)
WT	N_{Pi}	0.0012 ± 0.0006	1.983 ± 0.008	0.5 ± 1.0
	N_{Iz}	0.0011	2.214	
	S	0.002 ± 0.002	2.26 ± 0.01	
	C_{Pi}	0.002 ± 0.001	2.98	
			3.02 ± 0.01	
			3.06	
	Pi Multiple	0.002		
Y48*p*CMF	N_{Pi}	0.003 ± 0.001	1.990 ± 0.001	0.4 ± 1.3
	N_{Iz}	0.0011	2.21	
	S	0.003 ± 0.002	2.25 ± 0.01	
	C_{Pi}	0.002 ± 0.001	2.99	
			3.03 ± 0.02	
			3.06	
	Pi Multiple	0.003		

*The amplitude reduction factor, S_0^2, was set to 1.0 for all fits. Δk_{WT} = 1.389 ─ 11.885 Å^{-1}; $\Delta k_{Y48pCMF}$ = 1.358 ─ 11.685 Å^{-1}; ΔR_{WT} = 1.15 ─ 2.95 Å; $\Delta R_{Y48pCMF}$ = 1.18 ─ 2.95 Å. Fit *R* factors: R_{WT} = 0.0043; $R_{Y48pCMF}$ = 0.0097.

Table S4. Comprehensive ^{15}N relaxation parameters of the WT and Y48*p*CMF C*c* species

	WT C*c*	Y48*p*CMF C*c*	Difference
R_1 (s^{-1})	2.26 ± 0.08	2.15 ± 0.07	0.11
R_2 (s^{-1})	8.53 ± 0.46	9.14 ± 0.48	0.61
R_2 / R_1	3.77 ± 0.23	4.25 ± 0.23	0.48
NOE ratio	0.80 ± 0.03	0.80 ± 0.02	0.00
τ_c (ns)	6.33 ± 0.02	6.96 ± 0.02	0.63

Table S5. Equilibrium and thermodynamic parameters for the interaction of WT and Y48*p*CMF C*c* at the two binding sites of C*c*$_1$, as determined by ITC

	***Proximal* site**				***Distal* site**				
Protein couple	K_{D1} (μM)	ΔH_1 (kcal/mol)	$-T\Delta S_1$ (kcal/mol)	ΔG_1 (kcal/mol)	K_{D2} (μM)	ΔH_2 (kcal/mol)	$-T\Delta S_2$ (kcal/mol)	ΔG_2 (kcal/mol)	***n***
C*c* WT$_{red}$/C*c*$_{1red}$[a,1]	11.5	11.7	–18.40	–6.70	54.0	10.5	–16.30	–5.80	2
C*c* Y48*p*CMF$_{red}$/C*c*$_{1red}$[a]	5.1	–1.8	–5.42	–7.22	230.0	4.4	–9.36	–4.96	2
C*c* WT$_{ox}$/C*c*$_{1ox}$[b]	1.9	6.2	–14.00	–7.80	110.0	1.1	–6.50	–5.40	2
C*c* Y48*p*CMF$_{ox}$/C*c*$_{1ox}$[b]	1.8	8.2	–16.03	–7.83	71.0	3.3	–8.96	–5.66	2
C*c* WT$_{ox}$/C*c*$_{1ox}$[c]	50.0	4.3	–10.16	–5.86	140.0	0.8	–6.05	–5.25	2
C*c* Y48*p*CMF$_{ox}$/C*c*$_{1ox}$[c]	12.0	1.4	–8.11	–6.71	140.0	1.3	–6.55	–5.25	2

Relative errors: K_D, 20%; ΔH and $-T\Delta S$, 5%; ΔG 2%

[1] = Ref. 3

[a] = pH 7.4

[b] = pH 5.8

[c] = pH 8.5

Table S6. Equilibrium and thermodynamic parameters for the interaction of WT and Y48*p*CMF C*c* at the two binding sites of bovine C*c*O, as determined by ITC

	***Proximal* site**				***Distal* site**				
Protein couple	K_{D1} (μM)	ΔH_1 (kcal/mol)	$-T\Delta S_1$ (kcal/mol)	ΔG_1 (kcal/mol)	K_{D2} (μM)	ΔH_2 (kcal/mol)	$-T\Delta S_2$ (kcal/mol)	ΔG_2 (kcal/mol)	***n***
C*c* WT_{red}/C*c*O_{red}[1]	0.03	–6.6	–3.7	–10.3	0.30	–5.4	–3.5	–8.9	2
C*c* Y48*p*CMF_{red}/C*c*O_{red}	2.10	–6.3	–1.4	–7.7	7.00	–30.0	23.0	–7.0	2

Relative errors: K_D, 20%; ΔH and $-T\Delta S$, 5%; ΔG, 2%

[1] = Ref. 3.

SUPPLEMENTARY FIGURES

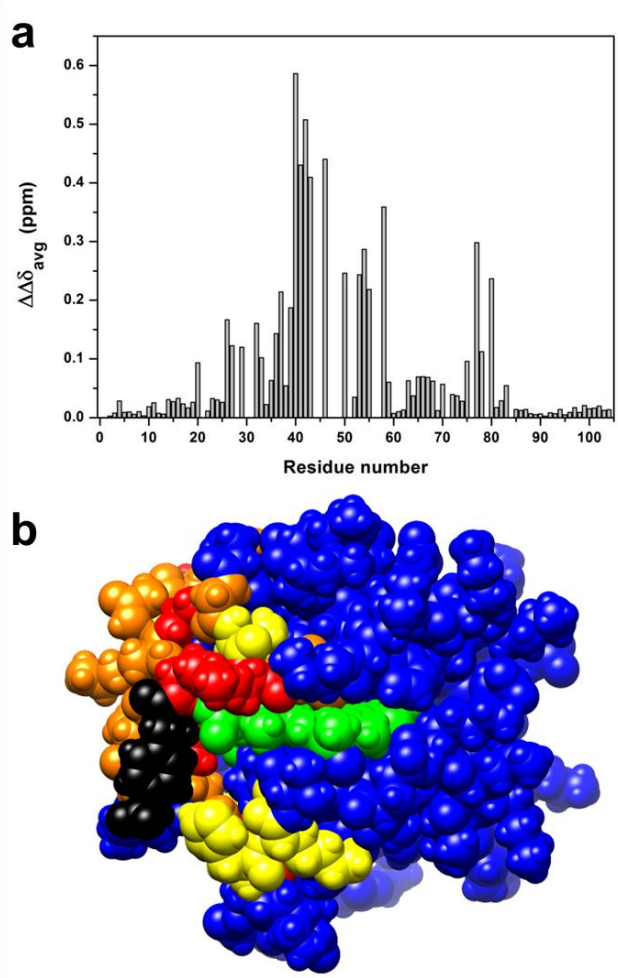

Figure S1. Chemical-shift differences between WT and Y48*p*CMF C*c*. (a) Plot of the chemical-shift differences between both C*c* species for backbone amides along their primary sequence. **(b)** The chemical shift differences are mapped on the Y48*p*CMF C*c* surface according to the degree of change. Residues are colored in yellow if the chemical-shift difference ranged between 0.1 and 0.2 ppm, and in red if the difference was greater than 0.2 ppm. Residues with undetectable backbone amide resonances in the ^{1}H-^{15}N HSQC spectrum of Y48*p*CMF C*c* but detectable in WT C*c* are colored in orange. *p*CMF48 and the heme group are given in black and green, respectively. Unaffected, unassigned and proline residues are in blue.

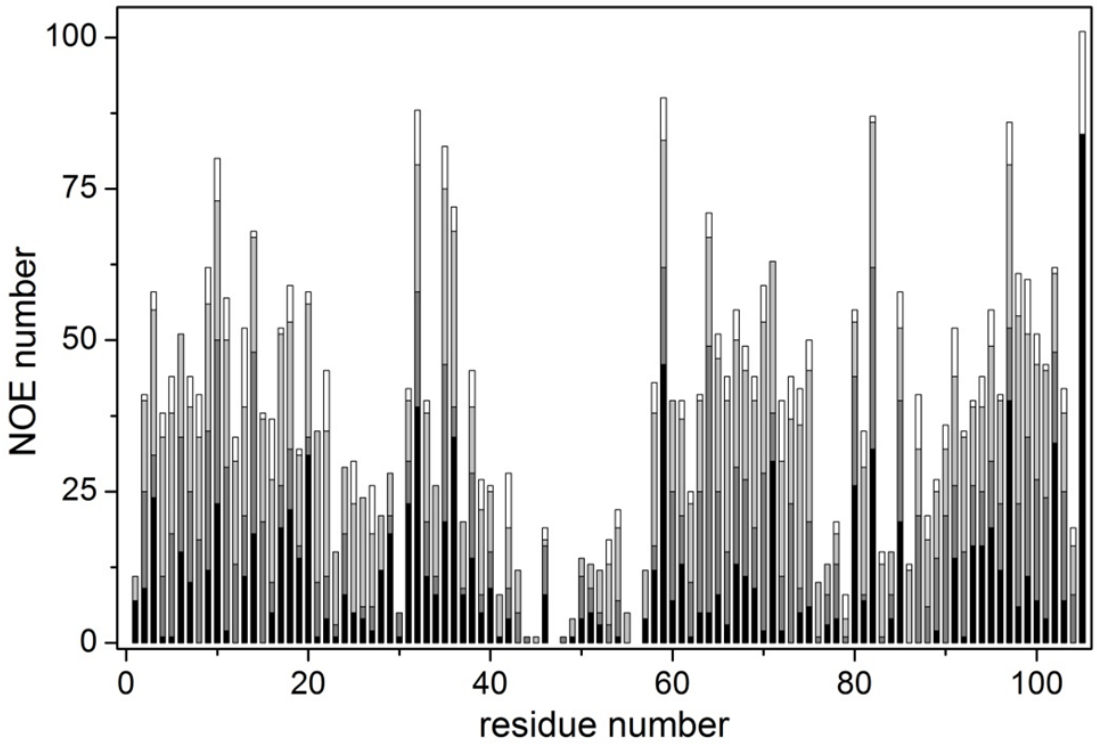

Figure S2. **Number of experimental meaningful NOEs per residue used for the structure calculation of Y48*p*CMF C*c*.** The color code for the NOE bars is: intra-residue, white; sequential, light gray; medium, gray; and long range, black. Residue 105 corresponds to the heme group.

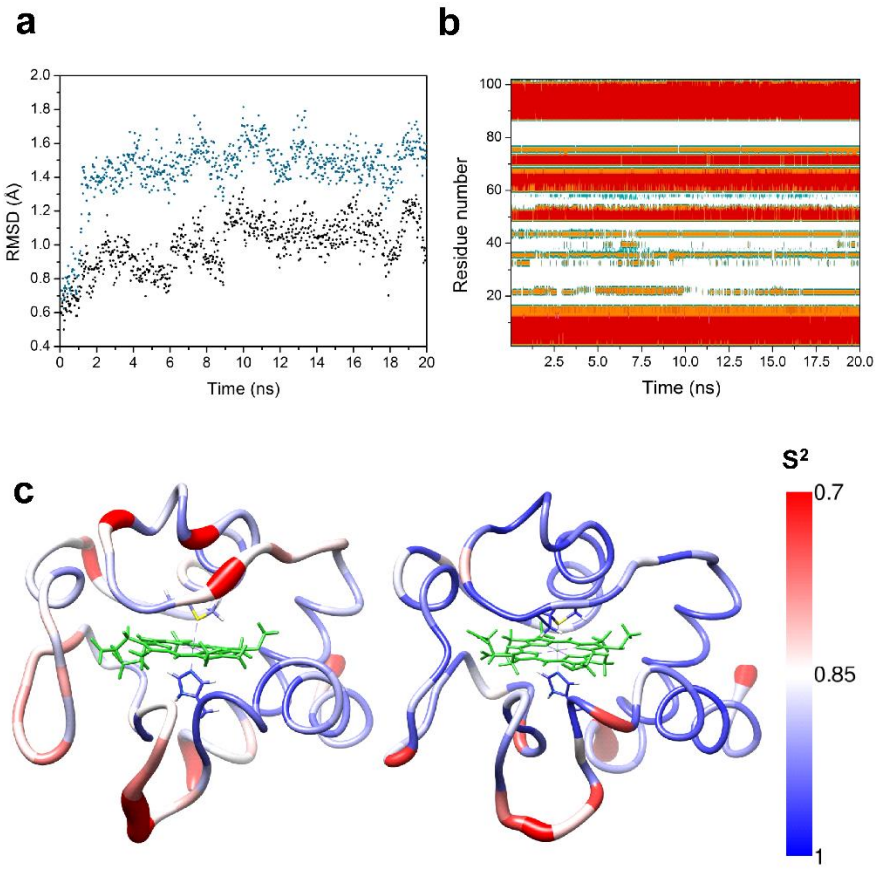

Figure S3. Molecular Dynamics simulations for the Y48*p*CMF variant and WT form of C*c*. (a) A non-restrained MD computation was performed to check the stability of conformers derived from the NMR structure of Y48*p*CMF C*c*. RMSD values are plotted along the full 20 ns trajectory, considering either residues away from the mutation surroundings (black) or the whole protein sequence (blue). **(b)** Time evolution of secondary structural elements along the MD trajectory represented in (**a**). The color code is as follows: α-helix, red; π-helix, orange; extended β-brand, blue; β-bridge, cyan; turn, yellow; and coil, white. **(c)** Comparison of S^2 order parameter values for Y48pCMF and WT C*c* obtained from MD computations. S^2 order parameter values per residue for Y48*p*CMF (*left*) and WT (*right*) C*c* are represented on their respective NMR ribbon structures using a blue-red scale (color key is shown). Heme atoms are in green. Heme axial ligands are also displayed. Internal mobility of alpha carbon atoms was calculated with the Amber software.

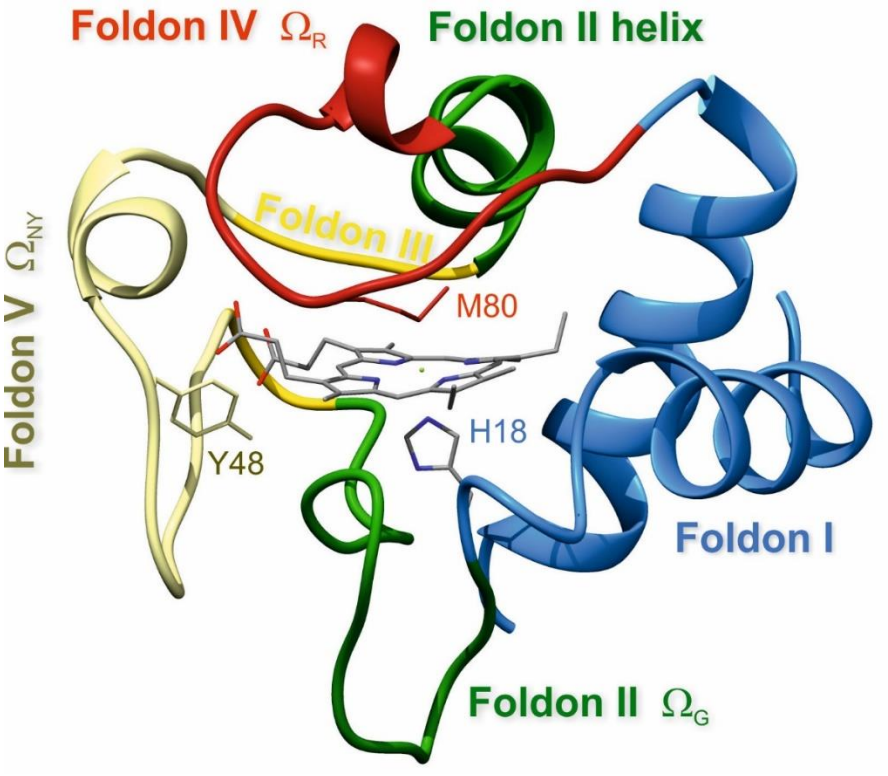

Figure S4: Folding units of WT C*c*. Ribbon diagram of human WT C*c* (PDB ID: 1J3S) (36), colored according to the foldon units schema by Maity and Eglander (44).

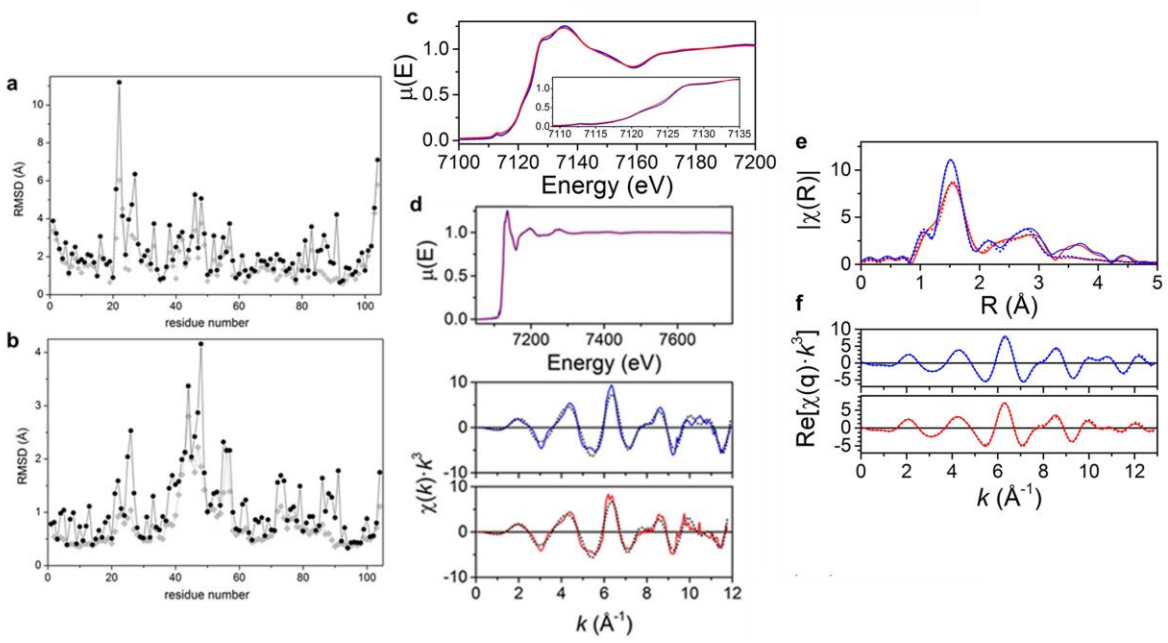

Figure S5. **NMR data in combination with XAS measurements. (a)** Per residue RMSD values between the first conformer of the NMR solution structures of WT C*c* (PDB ID: 1J3S) (36) and the refined lowest-TF Y48*p*CMF C*c*. Backbone and heavy atoms are represented as gray triangles and black circles, respectively. RMSD calculations were performed with the MOLMOL software (45). **(b)** Global RMSD values per residue of the best 20 conformers of Y48*p*CMF C*c* with respect to the mean structure. The color code is as in (**a**). **(c)** Overlay of the X-ray absorption near-edge structure (XANES) regions of the X-ray Absorption Spectra (XAS) spectra of reduced WT (blue) and Y48*p*CMF (red) C*c*. The *inset* displays an enlargement of the absorption edge. **(d)** Normalized XAS and Extended absorption fine Structure (EXAFS) waves of WT (blue) and Y48*p*CMF (red) C*c*. Black dots correspond to the best fits summarized in **Table S3**. **(e)** Modulus of the Fourier transforms of the EXAFS signals for the reduced WT (continuous line, blue) and Y48*p*CMF (continuous line, red) C*c* species. Dotted curves are the best fits of the experimental data carried out within the interval ΔR = 1.38–2.95 Å. **(f)** *q*-space, reverse Fourier transform of the experimental data (continuous lines) and best fits (dotted lines), following the same color-code as for **(e).**

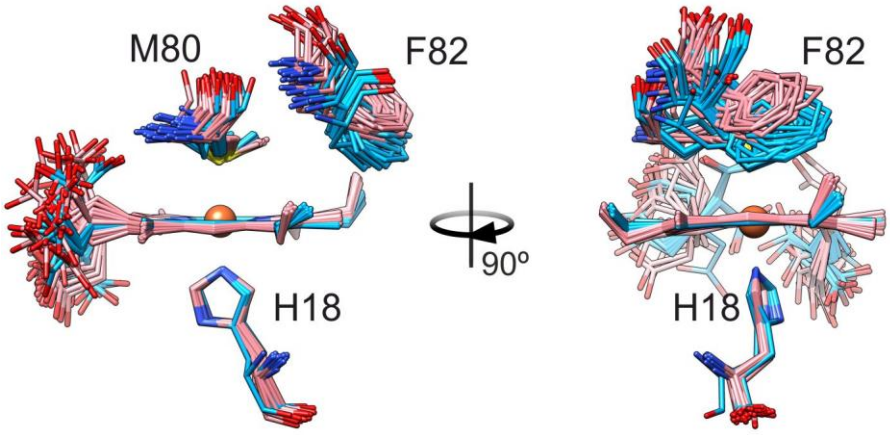

Figure S6. Relative orientation of Phe82 with respect to the heme moiety. The ensemble of the NMR structures from WT C*c* (PDB CODE: 1J3S) (36) and the Y48*p*CMF mutant (this work) are represented in sticks. Heavy atoms except carbons are in CPK colors, whereas carbons are colored in cyan and pink for the WT and mutant structures, respectively.

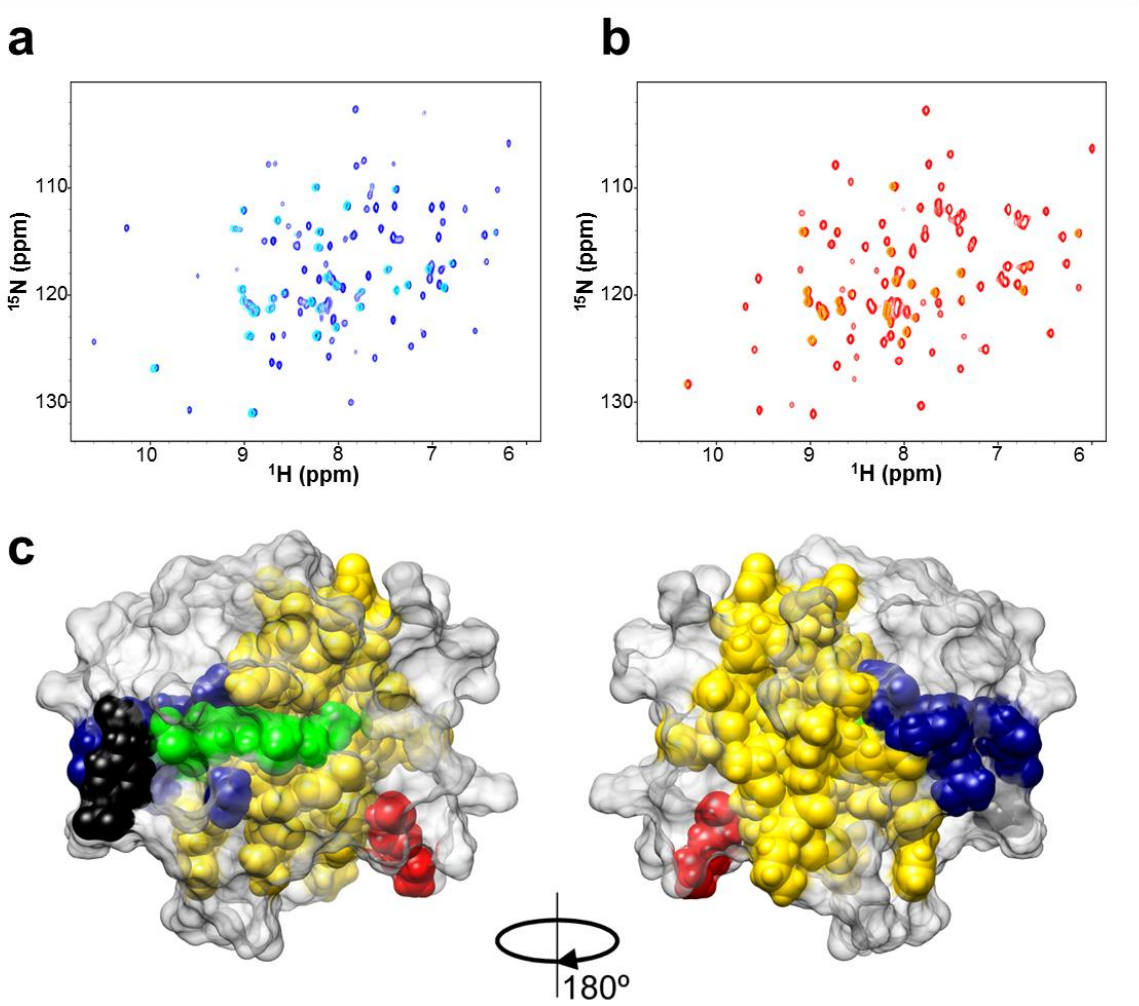

Figure S7. **Amide-hydrogen exchange experiments with WT and Y48*p*CMF C*c*. (a)** ^{1}H-^{15}N HSQC spectrum of WT C*c* recorded either in 95% H_2O and 5% D_2O (blue) or in 100% D_2O (cyan). **(b)** ^{1}H-^{15}N HSQC spectrum of Y48*p*CMF C*c* recorded either in 95% H_2O and 5% D_2O (red) or in 100% D_2O (gold). **(c)** Residues protected from amide-hydrogen exchange in both C*c* species are displayed in gold, those protected only in Y48*p*CMF C*c*, in red, and those protected only in WT C*c*, in blue. *p*CMF48 and the heme group are in black and green, respectively. The representation is projected on the Y48*p*CMF C*c* structure, whose surface is light gray.

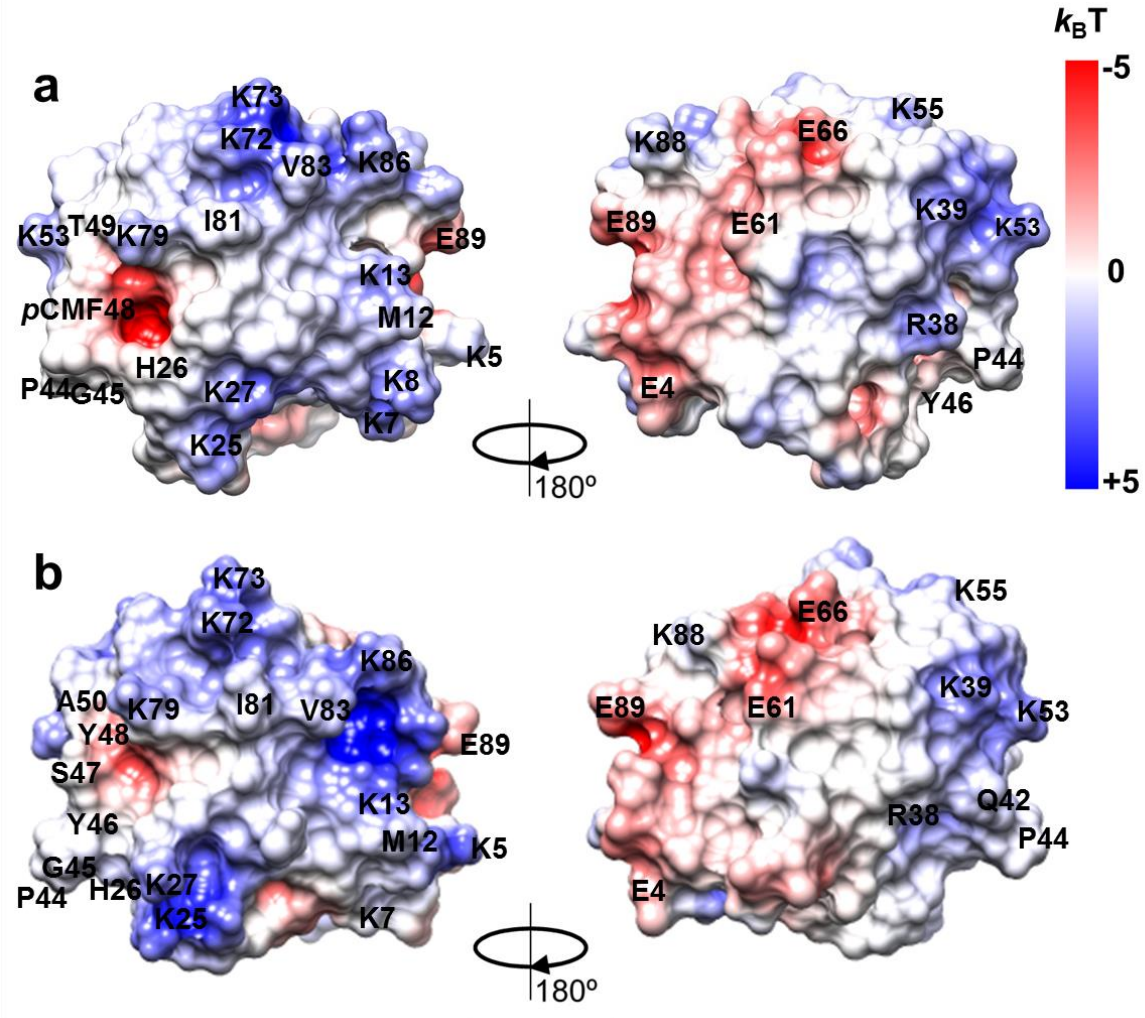

Figure S8. **(a**,**b) Surface electrostatic potentials of WT (a) and Y48*p*CMF (b) C*c* molecules.** Negatively and positively charged regions are depicted in red and blue, respectively. Simulations were performed with the DelPhi program (46) aided by Chimera (31), assuming an ionic strength of 250 mM. The color scale ranges from –5 (red) to +5 (blue) k_BT. Some residues were labelled to better show the orientation of both C*c* species. The PDB file 1J3S was used for the WT C*c* structure.

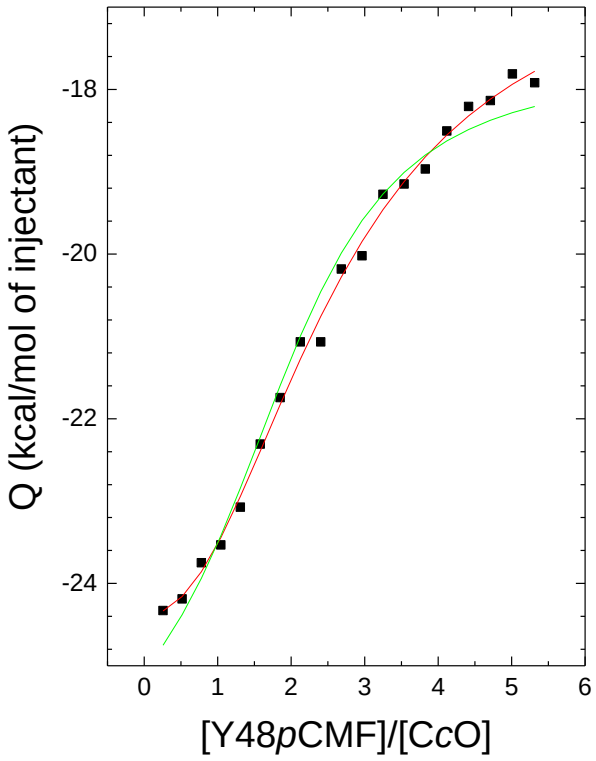

Figure S9. **ITC isotherms for the interaction of the Y48*p*CMF C*c* mutant with C*c*O.** Solid squares represent experimental data, which are fitted to a 2:1 model using either two identical (green) or different (red) K_D values.

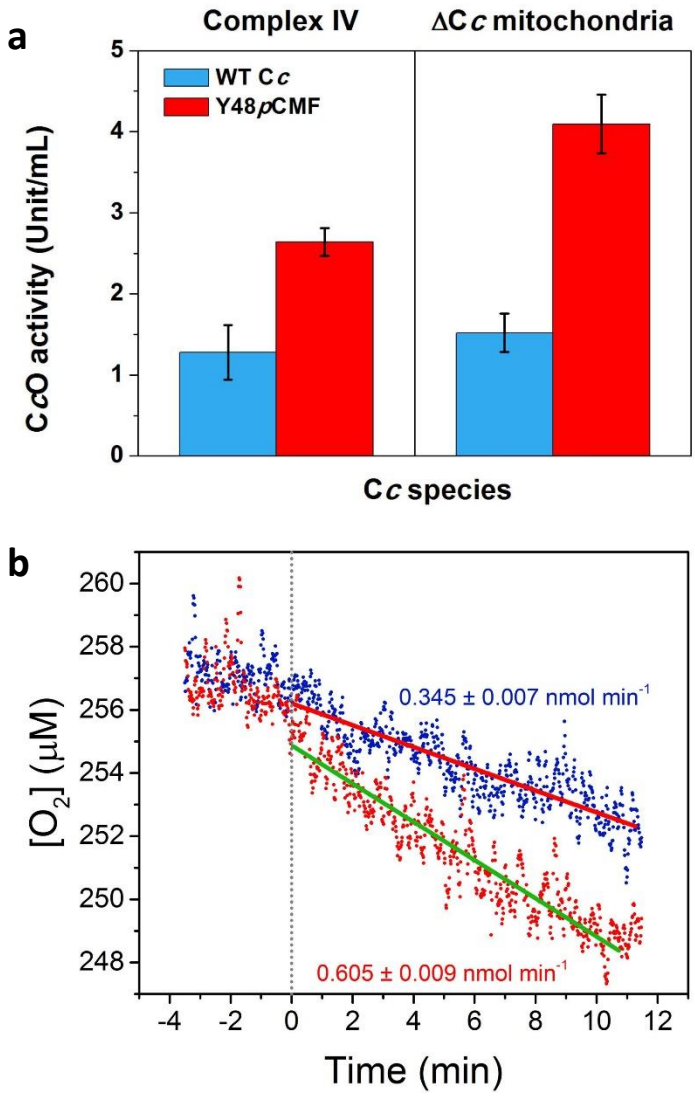

Figure S10. **Standard C*c*O assays. a)** Data in Figure 5a without normalization. C*c*O activities were measured by monitoring the absorption changes at 550 nm, as reported under Supplementary Methods. Activity units are μmol C*c* min^{-1}. **b)** Oxygen consumption under the experimental conditions used for the spectrophotometric assays. 1 mM sodium ascorbate was added to the reaction mixture. A control trace obtained with sodium ascorbate was subtracted from the experimental data, which are in blue and red for WT and mutant C*c*, respectively. The resulting oxygen consumption rates were calculated from the respective linear fit slopes.

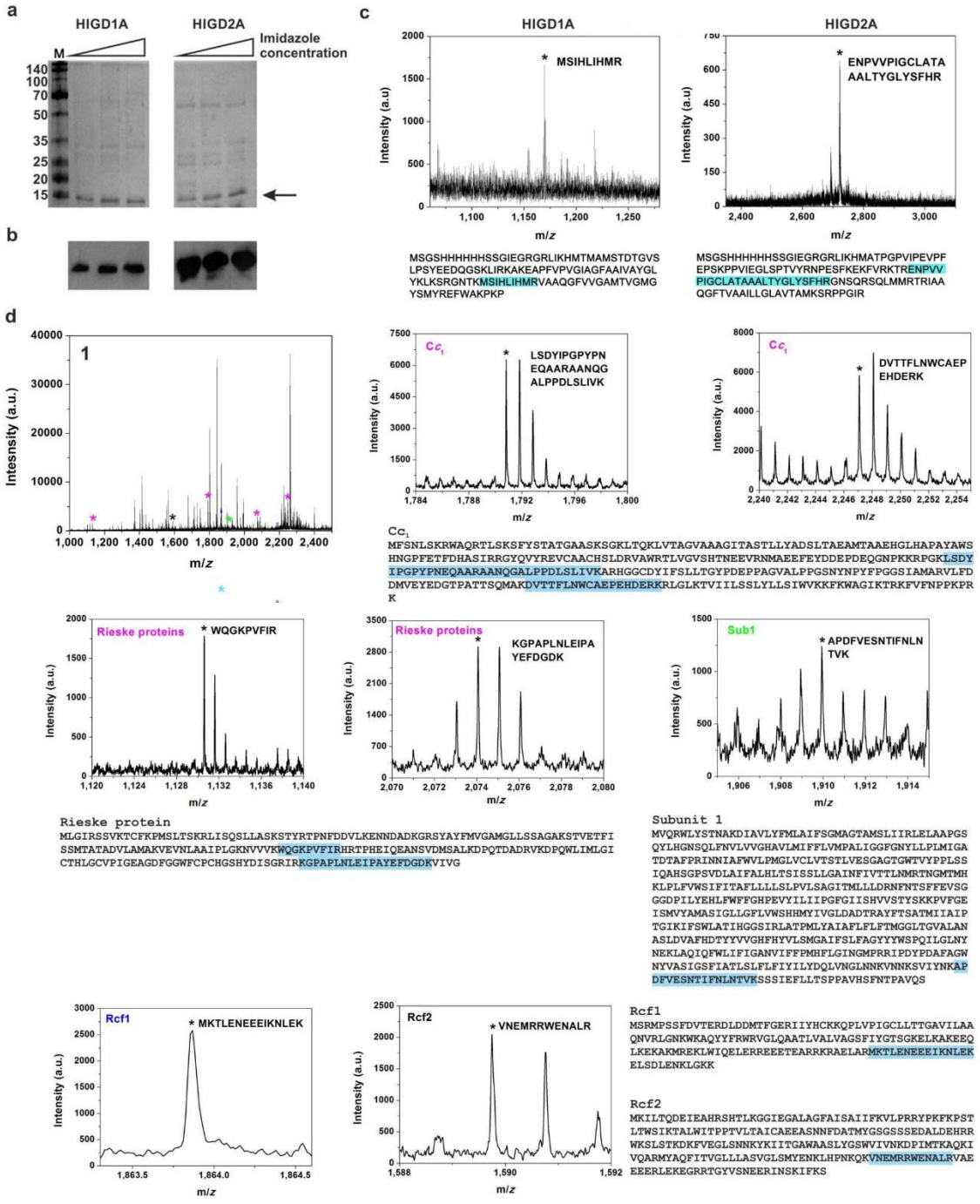

Figure S11. **HIGD proteins**. **(a)** SDS-PAGE of purified HIGD1A and HIGD2A His-tagged proteins after applying an imidazole gradient. M, molecular weight markers. The arrow points to the bands corresponding to HIGD proteins. **(b)** Western blot analysis using an antibody against His-tag to identify HIGD1A and HIGD2A following Ni-column purification. **(c)** Trypsin digestion of HIGD proteins followed by matrix-assisted laser desorption ionization with time-

of-light (MALDI-TOF) analysis. **(d)** Tryptic digestion of proteins from BN-PAGE bands followed by MALDI-TOF/TOF and highlighted by asterisks in Figure 5D. Specifically, the data presented here correspond to the upper band in YP-Gal in Figure 5D. The expected tryptic masses clearly matched the calculated values, with 0.5 Da tolerance. The sequence coverage of these fragments is shaded in cyan.

REFERENCES

1. Xie J, Supekova L, Schultz PG (2007) A genetically encoded metabolically stable analogue of phosphotyrosine in *Escherichia coli*. *ACS Chem Biol* 2: 474-478.
2. Guerra-Castellano A, *et al.* (2015) Mimicking tyrosine phosphorylation in human cytochrome *c* by the evolved tRNA synthetase technique. *Chem Eur J* 21: 15004-15012.
3. Moreno-Beltrán B, *et al.* (2015) Respiratory complexes III and IV can each bind two molecules of cytochrome *c* at low ionic strength. *FEBS Lett* 589: 476-483.
4. Moreno-Beltrán B, *et al.* (2014) Cytochrome c_1 exhibits two binding sites for cytochrome *c* in plants. *Biochim Biophys Acta – Bioenerg* 1837: 1717-1729.
5. Kelly SM, Jess TJ, Price NC (2005) How to study proteins by circular dichroism. *Biochim Biophys Acta – Proteins Proteomics* 1751: 119-139.
6. Sreerama N, Woody RM (2000) Estimation of protein secondary structure from circular dichroism spectra: comparison of CONTIN, SELCON, and CDSSTR methods with an expanded reference set. *Anal Biochem* 282: 252-260.
7. Greenfield NJ (2007) Using circular dichroism spectra to estimate protein secondary structure. *Nat Protoc* 1: 2876-2890.
8. Zuiderweg ER, Fesik SW (1988) Heteronuclear 3-dimensional NMR spectroscopy. A strategy for the simplification of homonuclear two-dimensional NMR spectra. *J Magn Reson* 78: 588-593.
9. Grzesiek S, Bax A (1993) Amino acid type determination in the sequential assignment procedure of uniformly $^{13}C/^{15}N$-enriched proteins. *J Biomol NMR* 3: 185-204.
10. Kay LE, Xu G, Singer AU, Muhandiram DR, Forman-Kay JD (1993) A gradient-enhanced HCCH-TOCSY experiment for recording side-chain ^{1}H and ^{13}C correlation in H_2O samples of proteins. *J Magn Reson* 101: 333-337.
11. Piotto M, Saudek V, Sklenar V (1991) Gradient-tailored excitation for single-quantum NMR spectroscopy of aqueous solutions. *J Biomol NMR* 2: 661-665.

12. Marion D, *et al.* (1989) Overcoming the overlap problem in the assignment of ^{1}H NMR spectra of larger proteins by use of three-dimensional heteronuclear ^{1}H-^{15}N Hartmann-Hahn-multiple quantum coherence and nuclear Overhauser-multiple quantum coherence spectroscopy: application to interleukin 1β. *Biochemistry* 28: 6150-6156.
13. Marion D, Kay LE, Sparks SW, Torchia DA, Bax A (1989). Three-dimensional heteronuclear NMR of nitrogen-^{15} labeled proteins. *J Am Chem Soc* 111: 1515-1517.
14. Zuiderweg ER, Fesik SW (1989) Heteronuclear three-dimensional NMR spectroscopy of the inflammatory protein C5a. *Biochemistry* 28: 2387-2391.
15. Kay LE, Torchia DA, Bax A (1989) Backbone dynamics of proteins as studied by ^{15}N inverse detected heteronuclear NMR spectroscopy: application to staphylococcal nuclease. *Biochemistry* 28: 8972-8979.
16. Blackledge M, Cordier F, Dosset P, Marion D (1998) Precision and uncertainty in the characterization of rotational diffusion from heteronuclear relaxation data. *J Am Chem Soc* 120: 4538-4539.
17. Dosset P, Hus JC, Blackledge M, Marion D (2000) Efficient analysis of macromolecular rotational diffusion from heteronuclear relaxation data. *J Biomol NMR* 16: 23-28.
18. Goddar TD, Kneller DG (2001) SPARKY 3, University of California, San Francisco, CA, USA.
19. Keller R (2004) The computer aided resonance assignment tutorial, 1st edn. CANTINA Verlag, Goldau, Switzerland.
20. Baistrocchi P, Banci L, Bertini I, Turano P (1996) Three-dimensional solution structure of *Saccharomyces cerevisiae* reduced iso-1-cytochrome *c*. *Biochemistry* 35: 13788-13796.
21. Bartels C, Xia TH, Billeter M, Guntert P, Wuthrich K (1995) The program XEASY for computer-supported NMR spectral analysis of biological macromolecules. *J Biomol NMR* 6: 1-10.

22. Güntert P, Mumenthaler C, Wüthrich K (1997) Torsion angle dynamics for NMR structure calculation with the new program Dyana1. *J Mol Biol* 273: 283-298.
23. Bartalesi I, Bertini I, Rosato A (2003) Structure and dynamics of reduced *Bacillus pasteurii* cytochrome *c*: oxidation state dependent properties and implications for electron transfer processes. *Biochemistry* 42: 739-745.
24. Banci L, *et al.* (1997) Solution structure of oxidized *Saccharomyces cerevisiae* iso-1-cytochrome *c*. *Biochemistry* 36: 8992-9001.
25. Assfalg M, *et al.* (2002) A quick solution structure determination of the fully oxidized double mutant K9-10A cytochrome c_7 from *Desulfuromonas acetoxidans* and mechanistic implications. *J Biomol NMR* 22: 107-122.
26. Duan Y, *et al.* (2003) A point-charge force field for molecular mechanics simulations of proteins based on condensed-phase quantum mechanical calculations. *J Comput Chem* 24: 1999-2012.
27. Case DA, *et al.* (2006) AMBER 9 University of California, San Francisco.
28. Andersen HC (1980) Molecular dynamics simulations at constant pressure and/or temperature. *J Chem Phys* 24: 1999-2012.
29. Ryckaert JP, Ciccotti G, Berendsen HJC (1977) Numerical integration of the cartesian equations of motion of a system with constraints: Molecular dynamics of *n*-Alkanes. *J Comp Phys* 23: 327-341.
30. Autenrieth F, Tajkhorshid E, Baudry J, Luthey-Schulten Z (2004) Classical force field parameters for the heme prosthetic group of cytochrome *c*. *J Comput Chem* 25: 1613-1622.
31. Pettersen EF, *et al.* (2004) UCSF Chimera - A visualization system for exploratory research and analysis. *J Comput Chem* 25: 1605-1612.
32. Bhattacharya A, Tejero R, Montelione GT (2007) Evaluating protein structures determined by structural genomics consortia. *Proteins* 66: 778-795.

33. Doreleijers JF, *et al.* (2012) CING: an integrated residue-based structure validation program suite. *J Biomol NMR* 54: 267-283.
34. Ravel B, Newville M (2005) ATHENA, ARTEMIS, HEPHAESTUS: data analysis for X-ray absorption spectroscopy using IFEFFIT. *J Synchrotron Rad* 12: 537-541.
35. Rajagopal BS, *et al.* (2013) The hydrogen-peroxide-induced radical behaviour in human cytochrome *c*-phospholipid complexes: implications for the enhanced pro-apoptotic activity of the G41S mutant. *Biochem J* 456: 441-452.
36. Jeng WY, Chen CY, Chang HC, Chuang WJ (2002) Expression and characterization of recombinant human cytochrome *c* in *E. coli*. *J Bioenerg Biomembr* 34: 423-431.
37. Serpas L, Milorey B, Pandiscia LA, Addison AW, Schweitzer-Stanner R (2016) Autoxidation of reduced horse heart cytochrome c catalyzed by cardiolipin-containing membranes. *J Phys Chem B* 120: 12219-12231.
38. Strogolova V, Furness A, Robb-McGrath M, Garlich J, Stuart RA (2012) Rcf1 and Rcf2, members of the hypoxia-induced gene 1 protein family, are critical components of the mitochondrial cytochrome bc_1-cytochrome *c* oxidase supercomplex. *Mol Cell Biol* 32: 1363-1373.
39. Padilla-López S. *et al.* (2009) Genetic evidence for the requirement of the endocytic pathway in the uptake of coenzyme Q6 in *Saccharomyces cerevisiae*. *Biochim Biophys Acta – Biomembr* 1788: 1238-1248.
40. Belikova NA, *et al.* (2006) Peroxidase activity and structural transitions of cytochrome *c* bound to cardiolipin-containing membranes. *Biochemistry* 45: 4998-5009.
41. Rodríguez-Roldán V, García-Heredia JM, Navarro JA, De la Rosa MA, Hervás M (2008) Effect of nitration on the physicochemical and kinetic features of wild-type and monotyrosine mutants of human respiratory cytochrome *c*. *Biochemistry* 47: 12371-12379.

42. Pecina P, *et al.* (2010) Phosphomimetic substitution of cytochrome *c* tyrosine 48 decreases respiration and binding to cardiolipin and abolishes ability to trigger downstream caspase activation. *Biochemistry* 49: 6705-6714.
43. Bradford MM (1976) A rapid and sensitive method for the quantitation of microgram quantities of protein utilizing the principle of protein-dye binding. *Anal Biochem* 72: 248-254.
44. Maity H, Maity M, Englander SW (2004) How cytochrome *c* folds, and why: submolecular foldon units and their stepwise sequential stabilization. *J Mol Biol* 34: 223-233.
45. Koradi R, Billeter M, Wüthrich K (1996) MOLMOL: a program for display and analysis of macromolecular structures. *J Mol Graph* 51: 29-32.
46. Nicholls A, Honig B (1991) A rapid finite difference algorithm, utilizing successive overrelaxation to solve the Poisson–Boltzmann equation. *J Comput Chem* 12: 435-445.